# Measurement of the p(e,e′π+)n reaction close to threshold and at low Q2

Friščić, Ivica; Achenbach, P.; Gayoso, C. Ayerbe; Baumann, D.; Böhm, R.; Bosnar, Damir; Debenjak, L.; Denig, A.; Ding, M.; Distler, M.O.; ...

# Measurement of the $p(e, e'\pi^+)n$ reaction close to threshold and at low $Q^2$

I. Friščić [a,*,1], P. Achenbach [b], C. Ayerbe Gayoso [b], D. Baumann [b], R. Böhm [b], D. Bosnar [a], L. Debenjak [c], A. Denig [b], M. Ding [b], M.O. Distler [b], A. Esser [b], H. Merkel [b], D.G. Middleton [b], M. Mihovilovič [b,c], U. Müller [b], J. Pochodzalla [b], B.S. Schlimme [b], M. Schoth [b], F. Schulz [b], C. Sfienti [b], S. Širca [d,c], M. Thiel [b], Th. Walcher [b]

[a] *Department of Physics, Faculty of Science, University of Zagreb, HR-10002 Zagreb, Croatia*
[b] *Institut für Kernphysik, Johannes Gutenberg-Universität, D-55099 Mainz, Germany*
[c] *Jožef Stefan Institute, SI-1000 Ljubljana, Slovenia*
[d] *Department of Physics, University of Ljubljana, SI-1000 Ljubljana, Slovenia*

ARTICLE INFO

ABSTRACT

The cross section of the $p(e, e'\pi^+)n$ reaction has been measured for five kinematic settings at an invariant mass of $W = 1094$ MeV and for a four-momentum transfer of $Q^2 = 0.078$ $(\text{GeV}/c)^2$. The measurement has been performed at MAMI using a new short-orbit spectrometer (SOS) of the A1 collaboration, intended for detection of low-energy pions. The transverse and longitudinal cross section terms were separated using the Rosenbluth method and the transverse-longitudinal interference term has been determined from the left-right asymmetry. The experimental cross section terms are compared with the calculations of three models: DMT2001, MAID2007 and $\chi$MAID. The results show that we do not yet understand the dynamics of the fundamental pion.

## 1. Introduction

Pion electroproduction on protons near threshold has been in the focus of both theoretical and experimental research for more than four decades. The pioneering theoretical studies were performed by deriving low-energy theorems (LETs) based on chirality conservation for soft pions, which established the connection between the S-wave transverse multipole of the charged pion electroproduction and the axial form factor [1,2]. The same result was later derived in the framework of current algebra using the partially conserved axial current (PCAC) and, additionally, a relation between the S-wave longitudinal multipole and the induced pseudoscalar form factor was derived [3]. After the formulation of chiral perturbation theory ($\chi$PT) new calculations showed [4,5] that the pion loop contributions to the LETs could not be neglected as it was the case in previous approaches [6,7].

Compared to the comprehensive experimental data for pion photoproduction [8–10] (and references therein), the existing data for electroproduction, i.e., at non-vanishing four-momentum transfer, are sparse. This is especially true for the charged pion channel close to threshold, where detection of either a recoiling neutron or a pion at low energy makes a measurement difficult. The earliest charged pion electroproduction experiments were carried out in the 1970s, but their results had large statistical and systematic uncertainties. They can be divided into single arm experiments as in Stanford (SLAC) [11] and Kharkov [12], or double arm coincidence electron and neutron experiments as in Frascati [13], Hamburg (DESY) [14,15] and Daresbury [16,17]. From the 1990s and onwards, electron and pion coincidence experiments were performed in Saclay [18], JLab (CLAS) [19] and in Mainz (MAMI) [20, 21].

In the one-photon-exchange approximation, the differential cross section of the $p(e, e'\pi^+)n$ reaction can be expressed as a product of the virtual photon flux $\Gamma$ and the virtual photon cross section $d\sigma_v/d\Omega_\pi^\star$ [3,22]. For an unpolarised electron beam and an unpolarised target, $d\sigma_v/d\Omega_\pi^\star$ can be further factorized into one transverse ($T$), one longitudinal ($L$) and two interference ($TL$ and $TT$) terms (convention from [10]):

$$\frac{d\sigma_v}{d\Omega_\pi^\star} = \frac{d\sigma_T}{d\Omega_\pi^\star} + \epsilon\frac{d\sigma_L}{d\Omega_\pi^\star} + \sqrt{2\epsilon(1+\epsilon)}\frac{d\sigma_{TL}}{d\Omega_\pi^\star}\cos\phi_\pi$$

$$+ \epsilon\frac{d\sigma_{TT}}{d\Omega_\pi^\star}\cos 2\phi_\pi \qquad (1)$$

$$\epsilon = \left(1 + \frac{2\vec{q}^2}{Q^2}\tan^2\frac{\theta_{e^-}}{2}\right)^{-1}$$

where $\phi_\pi = \phi_\pi^\star$ is the angle between the scattering and the reaction plane, the asterisk denotes quantities evaluated in the hadronic centre-of-mass frame. $\epsilon$ is the transverse polarization of the virtual photon and at fixed $Q^2$ the value of $\epsilon$ can be selected by using the right combination of beam energy and electron scattering angle $\theta_{e^-}$. The $T$ and the $L$ terms can be separated by a measurement in the so-called parallel kinematics (the pion production angle $\theta_\pi = \theta_\pi^\star = 0°$). There, the interference terms vanish due to their angular dependence, $d\sigma_{TL} \sim sin\theta_\pi^\star$ and $d\sigma_{TT} \sim sin^2\theta_\pi^\star$ [3,22]. The virtual photon cross section is determined for fixed values of the invariant mass $W$ and four-momentum transfer $Q^2$, by varying only $\epsilon$. The separation of $T$ and $L$ terms is then performed using the Rosenbluth method [23]. The determination of the $TL$ term requires two measurements at fixed values of $W$, $Q^2$, $\epsilon$ and $\theta_\pi^\star \neq 0$. One measurement is performed at $\phi_\pi = 0°$ and the other at $\phi_\pi = 180°$ [22]. The $TL$ term can then be determined from the left-right asymmetry:

$$\frac{d\sigma_{TL}}{d\Omega_\pi^\star} = \frac{\left.\frac{d\sigma}{d\Omega_\pi^\star}\right|_{\phi_\pi=0°,\theta_\pi^\star\neq 0°} - \left.\frac{d\sigma}{d\Omega_\pi^\star}\right|_{\phi_\pi=180°,\theta_\pi^\star\neq 0°}}{2\sqrt{2\epsilon(1+\epsilon)}} \qquad (2)$$

Knowing the precise values of the experimental cross section terms $T$, $L$ and $TL$ at a given $W$ and $Q^2$ allows the testing of the theoretical predictions of these quantities, which in turn are based on various approaches in describing the structure of the nucleon.

Experiments in Mainz were performed at 46 MeV above the production threshold, using the high precision spectrometer setup of the A1 Collaboration [24]. Since the particle path in these spectrometers is of the order of 10 m, in an experiment closer to threshold most pions would decay before reaching detectors. This would lead to contamination of the data with muons indistinguishable from pions, thus increasing systematic errors beyond acceptable limits. A spectrometer with a shorter path significantly reduces the muon contamination.

In this Letter we present the measurement and analysis of a $p(e, e'\pi^+)n$ coincidence experiment at only 15 MeV above the threshold. The experiment was performed at a fixed invariant mass of $W = 1094$ MeV and virtual photon four-momentum transfer of $Q^2 = 0.078$ $(GeV/c)^2$. The low-energy pions were detected in a new short-orbit spectrometer (SOS, see Fig. 1) [25] with a particle path of $\approx 1.6$ m. The obtained $T$, $L$ and $TL$ terms were compared with predictions of three different models.

## 2. Experiment

The experiment was carried out at the spectrometer setup of the A1 Collaboration [24] at the Mainz Microtron [26]. The energy of the unpolarised electron beam was varied between 345 and 855 MeV. The beam current ranging from 7 to 25 μA was measured using a flux-gate magnetometer. A cylindrical target cell with a diameter of 2 cm and Havar walls of 50 μm was used in combination with a high power liquid hydrogen cooling system. In order to avoid density fluctuations, the beam was rastered in transversal directions and the liquid hydrogen was recirculated.
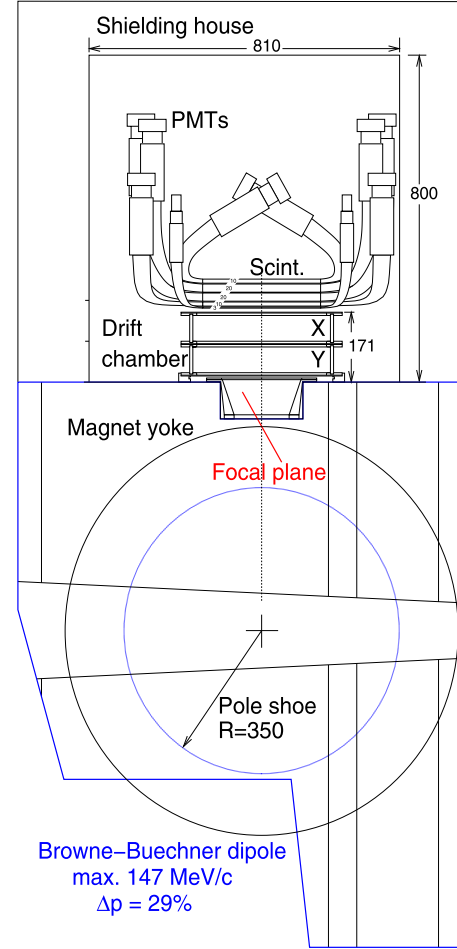


**Fig. 1.** (Colour online.) The SOS spectrometer with the detector system. The measures are in mm, the target position is 1131.6 mm to the right in line with the central cross.

**Table 1**
Central values of the kinematic settings: $E$ is the energy of the beam, $p_{e^-}$ is the momentum of the scattered electron, $\theta_{e^-}$ is the angle of the scattered electron, $p_{\pi^+}$ is the momentum of the pion and $\theta_{\pi^+}$ is the pion production angle.

| Setting | $\epsilon$ | $E$ (MeV) | $p_{e^-}$ (MeV/c) | $\theta_{e^-}$ (°) | $p_{\pi^+}$ (MeV/c) | $\theta_{\pi^+}$ (°) |
|---------|-----------|-----------|-------------------|--------------------|---------------------|----------------------|
| 1 | 0.3065 | 345 | 134.8 | 80.7 | 113 | 22.40 |
| 2 | 0.5913 | 450 | 239.8 | 50.3 | 113 | 31.79 |
| 3 | 0.8970 | 855 | 644.8 | 22.5 | 113 | 42.94 |
| 4 | 0.8970 | 855 | 644.8 | 22.5 | 110 | 32.80 |
| 5 | 0.8970 | 855 | 644.8 | 22.5 | 110 | 53.10 |

The scattered electron was detected in the standard spectrometer A, while the produced charged pion was measured with the SOS. In the electron arm, four vertical drift chambers were used for particle tracking, while in the pion arm the tracking detector was realized with two volume type drift chambers using a helium-ethane mixture as counting gas. In both arms, scintillation detectors were used for trigger and timing purposes, and additionally, they were used for particle identification in the pion arm. The angular acceptances of the spectrometers were defined by heavy metal collimators: 21 msr for spectrometer A and 2 msr for the SOS. The momentum acceptance was 20% and 29% in spectrometer A and SOS, respectively.

The kinematic settings are summarized in Table 1. The settings 1, 2 and 3 were measured in parallel kinematics for the separation
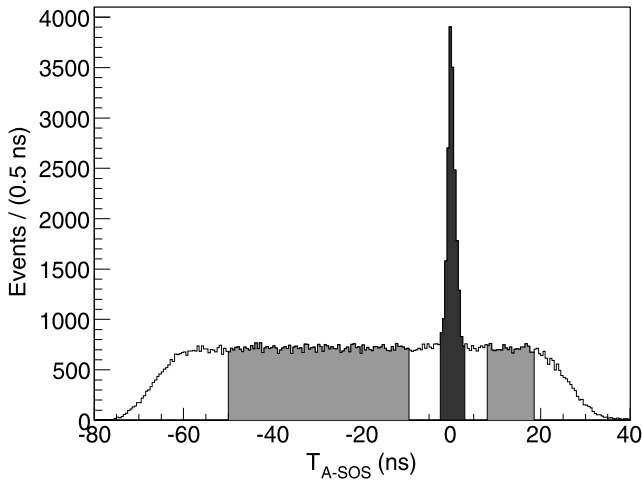
**Fig. 2.** Coincidence time distribution. The dark gray area includes the true coincidences and the light gray area contains only random coincidence events used for the background estimation.

of $T$ and $L$ terms. The last two settings were measured at $\theta_\pi^\star = \pm 18.7°$ with respect to the virtual photon direction, to determine the $TL$ term.

## 3. Data analysis

The true events were first identified by measuring the coincidence time between spectrometer A and SOS, which was corrected for the path length of the particle in the corresponding spectrometer and for delays in the electronics. After these corrections, a sharp coincidence peak of 2.8 ns FWHM was obtained, see Fig. 2. A cut at $-2$ ns $\leq \Delta t \leq 2.5$ ns was used on the coincidence peak to select the true electron-pion pairs. Cuts on sidebands at $-50$ ns $\leq \Delta t \leq -10$ ns and 7 ns $\leq \Delta t \leq 18$ ns were used to estimate the background contribution from random coincidences. In the case of spectrometer A, further reduction of the background was achieved by cuts on the reconstructed electron momentum and the reconstructed vertex. For the SOS, this included cuts on acceptance of the dispersive angle and reconstructed pion momenta. A special cut and correction was applied for particles passing very close to the signal wires of the SOS drift chamber [25] which affected approx. 2% of the events.

The measured electron and pion momenta were used to calculate the missing mass of an unobserved neutron for each event. Additionally, particle momentum was corrected for energy loss in the target and in different materials. The random coincidence background was removed by subtraction. As an example, the resulting missing mass distribution of setting 2 is shown in Fig. 3. Events between $-3$ and $11$ MeV/$c^2$ relative to the neutron mass were selected as the final true events. These events were corrected for detector inefficiencies (varying from 16.2% to 21.0%) as well as for in-flight pion decay. The calculation of the decay correction factor was based on the determined pion trajectory length from the interaction vertex to the scintillation detectors and the measured pion momentum.

Integrated luminosity was calculated off-line and corrected for dead time (varying from 5.4% to 7.8%). The target density value was updated if the temperature changed by more than 0.03 K and the pressure by more than 2 mbar, whereas smaller fluctuations were averaged out.

The phase space accepted by the apparatus was determined based on a Monte Carlo simulation, which provided event by event corrections stemming from radiative (internal and external
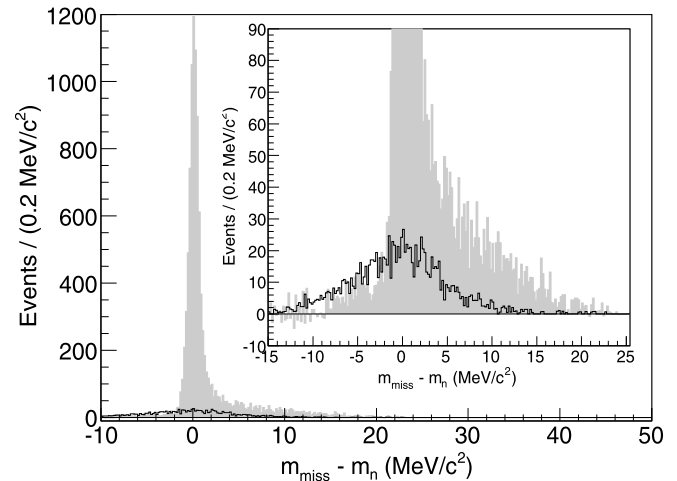


**Fig. 3.** The background subtracted missing mass distribution of setting 2 relative to the neutron mass (light gray). The insert shows the plot in the peak region at a magnified scale. The black line denotes the muon distribution from the simulation of the pion decay.
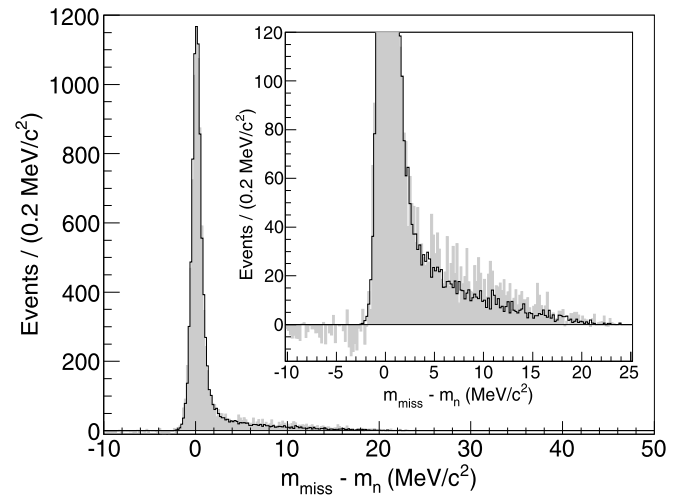


**Fig. 4.** Missing mass distribution of setting 2 (light gray) with the muon distribution subtracted. The insert shows the radiative tail region at a magnified scale. The black line represents the distribution of the accepted phase space for setting 2. Experimental and simulated were made comparable by requesting that the highest bins of both distributions have the same value.

Bremsstrahlung, vertex correction) and ionization losses, and also included the angular and momentum resolution parameters of the spectrometers. Muons originating from in-flight pion decays, created near the detectors or close to the direction of the decayed pions, were detected and a certain amount of these could not be distinguished from pions. Therefore, a Monte Carlo simulation of pion decays inside the SOS was performed. The simulation incorporated full tracking of a pion or produced muon trajectory from the vertex, through the simulated magnetic field of the SOS dipole magnet, to the scintillation detectors. In order to make distributions form the experiment and simulation comparable, the muon distribution was normalized with the ratio of the highest bins of the experimental distribution and the combined simulated pion + muon distribution. Fig. 3 (insert) shows the muon missing mass distribution (denoted by a black line). As expected, muons under the true events distribution (shaded light gray) will be misidentified as pions. Furthermore, the shape of the muon distribution follows the "foot" at the left edge of the true events distribution.

**Table 2**
Individual systematic uncertainties.

| Source | Relative uncertainty (%) |
|---|---|
| Layer of residual gases | 0.10 |
| Phase space | 0.12 |
| Muon contamination | 0.23 |
| Pion decay correction | 0.54 |
| Luminosity | 0.58–0.59 |
| Badly reconstructed tracks (SOS) | 0.68 |
| Missing mass cut | 2.44–3.20 |
| All other cuts | 0.96 |
| Total (quadrature sum) | 2.9–3.5 |

**Table 3**
Measured $p(e, e'\pi^+)n$ cross sections.

| Setting | $d\sigma/d\Omega^\star_\pi$ ($\mu$b/sr) | $\pm$ | Total error ($\mu$b/sr) | Stat. error ($\mu$b/sr) | Syst. error ($\mu$b/sr) |
|---|---|---|---|---|---|
| 1 | 4.91 | $\pm$ | 0.15 (3.1%) | 0.06 (1.2%) | 0.14 (2.9%) |
| 2 | 5.73 | $\pm$ | 0.21 (3.7%) | 0.06 (1.1%) | 0.20 (3.5%) |
| 3 | 6.83 | $\pm$ | 0.24 (3.5%) | 0.08 (1.2%) | 0.23 (3.4%) |
| 4 | 5.37 | $\pm$ | 0.18 (3.4%) | 0.05 (0.9%) | 0.17 (3.1%) |
| 5 | 8.53 | $\pm$ | 0.27 (3.2%) | 0.07 (0.8%) | 0.26 (3.1%) |

Naive subtraction of the muon distribution removes this structure and assures that the left edge of the experimental distribution agrees with the left edge of the phase space distribution (see Fig. 4). This confirms that the "foot" is caused by muons. Due to low statistics of the experimental data in the "foot" region, the subtraction introduces unphysical negative values in the experimental distribution. To avoid this when calculating the cross section, but also to prevent possible normalization issues, muons are not removed from experimental data using subtraction. Instead the muon percentage inside a certain missing mass interval is calculated based on simulation. For the missing mass interval from $-3$ to $11$ MeV/$c^2$ a muon contamination varying from 7.3% to 7.8% was obtained.

Table 2 contains individual and total relative systematic uncertainties. Given that we used a cryogenic target, a layer of residual gases formed on the target surface due to the non-perfect vacuum. The contribution of this layer was estimated by changing its thickness in the simulation. Contributions due to phase space and muon contamination were determined by simulation. The uncertainty of the pion decay correction was contributed by the errors of trajectory length and reconstructed pion momentum. Luminosity uncertainty comprises errors stemming from target density fluctuations, measurement of beam current and determination of the average target length. The fraction of corrected events per drift cell was used to estimate the contribution from badly reconstructed tracks. The main systematic uncertainty is due to the cut-off on the radiative tail of the missing mass distribution. This contribution depends on corrections for radiative processes which were applied in the simulations, the subtraction of the random background and the fluctuation of the data due to low statistics in the radiative tail (see Fig. 4 insert).

## 4. Results and discussion

Measured cross sections of the $p(e, e'\pi^+)n$ reaction, with the statistical, systematic and total errors, are listed in Table 3. The $L$ and $T$ terms (see Table 4) were extracted by performing a weighted linear regression on settings 1, 2, and 3, using the total errors as weights. The $TL$ term and corresponding total error were determined from the left–right asymmetry and Eq. (2).

**Table 4**
Experimental and model results for the $L$, $T$ and $TL$ terms of the charged pion electroproduction on protons at $W = 1094$ MeV and at $Q^2 = 0.078$ (GeV/$c$)$^2$.

| Term | Data $\pm$ Total error ($\mu$b/sr) | DMT2001 ($\mu$b/sr) | MAID2007 ($\mu$b/sr) | $\chi$MAID ($\mu$b/sr) |
|---|---|---|---|---|
| $T$ | $3.91 \pm 0.26$ (6.7%) | 4.38 | 4.39 | 4.73 |
| $L$ | $3.20 \pm 0.47$ (14.7%) | 3.33 | 4.22 | 2.89 |
| $TL$ | $-0.86 \pm 0.09$ (10.5%) | $-0.79$ | $-0.98$ | $-1.11$ |

The experimental terms are compared with predictions given by three state-of-the-art theoretical models [27]. The first model is the Dubna–Mainz–Taipei (DMT2001). The calculations were done within a meson-exchange dynamical model, which uses potentials derived from an effective chiral Lagrangian [28–32]. The second model is based on a partial-wave analysis using the Mainz unitary isobar model MAID2007 [10]. The third model is the Chiral MAID ($\chi$MAID) [33,34]. It calculates the pion photo- and electroproduction based on Lorentz-invariant baryon chiral perturbation theory up to and including order $q^4$. The low-energy constants (LECs) are fixed by fitting the previous experimental data in all available reaction channels. For this Letter, the LECs were not changed.

The obtained experimental results and model predictions for the $L$, $T$ and $TL$ cross section terms are presented in Table 4. The errors are the so called uncorrelated errors, better called one-parameter errors (see Chap. 9 of ref. [35]). The deviation of the theoretical values from the experimental results is of the order of one to three standard deviations of these errors customarily taken. However, these errors feign an agreement which does not exist. If one includes the correlation between the $T$ and the $L$ terms one can construct a 3d-error ellipsoid. The distance between the experimental values and the model predictions, using the principle axes of the error ellipsoid as a coordinate system, is a measure of the simultaneous agreement between the theoretical terms and the experiment. One gets a p-value of $2 \times 10^{-5}$ for the DMT2001 model, $6 \times 10^{-10}$ for $\chi$MAID, and $< 10^{-16}$ for MAID2007. The DMT2001 model has some edge over the others. It is based on a realistic pion–nucleon interaction and includes chiral symmetry from the start. Compared to $\chi$PT, the dynamic approach takes all loops up to the arbitrary order into account [30]. This makes it superior with respect to any $\chi$PT calculation. On the other hand, the predictions of $\chi$MAID depend strongly on LECs which are fixed by only few experimental results [33]. Adding of our results would lead to estimates of different LEC values, which may in turn better reproduce our $T$, $L$ and $TL$ terms.

Fig. 5 shows plots of models and the new results reported here, measured at $W = 1094$ MeV, and the previous MAMI measurements at $W = 1125$ MeV [20,21]. Even for the previous MAMI results, DMT2001 is overall in better agreement with the experiment, compared to the other two models. The same was also concluded from our terms. $\chi$MAID describes very well the T term data points of the previous MAMI results, better than MAID2007, but this is not a surprise since the used LECs were obtained by fitting the $W = 1125$ MeV data [33]. This situation is reversed for our data. The TL terms are better described by MAID2007 than by $\chi$MAID. Both models have difficulties in describing the L term data points of the previous MAMI results, but for the new data $\chi$MAID performs better.

At threshold and with the small momentum transfers in this experiment, chiral symmetry and its breaking should be a good framework for models. Therefore, our result is a clear challenge for theory. In view of the fundamental importance of the pion in hadron and nuclear physics a new effort is needed.
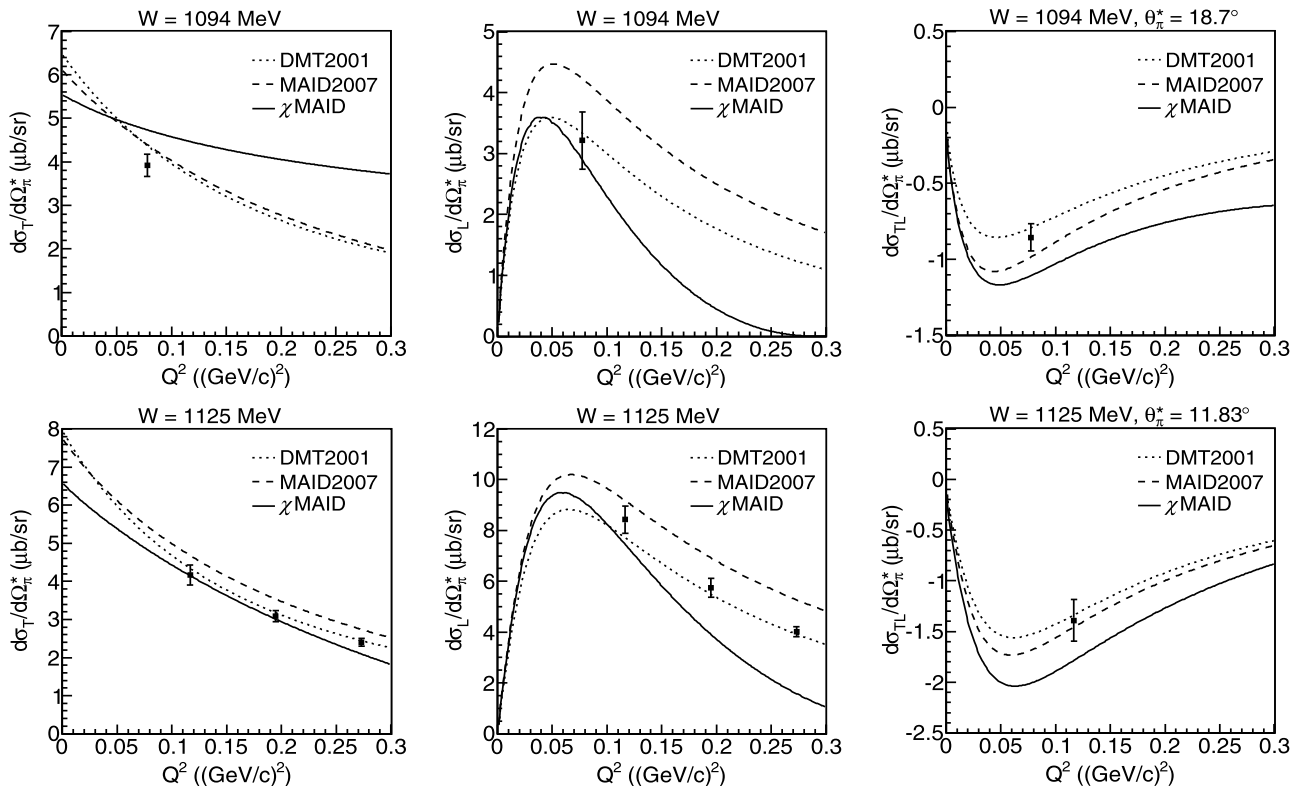
**Fig. 5.** Experimental T, L and TL terms with the total errors plotted together with model predictions as a function of $Q^2$. The figures in the first row show results at $W = 1094$ MeV, reported in this Letter. The second row shows previously published results from experiments at MAMI, measured at $W = 1125$ MeV [20,21].

## Acknowledgements

## References

[1] Y. Nambu, D. Lurié, Phys. Rev. 125 (1962) 1429, http://dx.doi.org/10.1103/PhysRev.125.1429.

[2] Y. Nambu, E. Shrauner, Phys. Rev. 128 (1962) 862, http://dx.doi.org/10.1103/PhysRev.128.862.

[3] E. Amaldi, S. Fubini, G. Furlan, Pion Electroproduction, Springer Tracts in Modern Physics, vol. 83, Springer, Berlin, 1979.

[4] V. Bernard, N. Kaiser, U.-G. Meissner, Phys. Rev. Lett. 69 (1992) 1877, http://dx.doi.org/10.1103/PhysRevLett.69.1877.

[5] V. Bernard, N. Kaiser, T.-S.H. Lee, U.-G. Meissner, Phys. Rev. Lett. 70 (1993) 387, http://dx.doi.org/10.1103/PhysRevLett.70.387.

[6] A.I. Vainshtein, V.I. Zakharov, Nucl. Phys. B 36 (1972) 589, http://dx.doi.org/10.1016/0550-3213(72)90238-6.

[7] S. Scherer, J.H. Koch, Nucl. Phys. A 534 (1991) 461, http://dx.doi.org/10.1016/0375-9474(91)90456-G.

[8] R.A. Arndt, et al., Phys. Rev. C 74 (2006) 045205, http://dx.doi.org/10.1103/PhysRevC.74.045205.

[9] D. Rönchen, et al., Eur. Phys. J. A 49 (2013) 44, http://dx.doi.org/10.1140/epja/i2013-13044-5.

[10] D. Drechsel, S.S. Kamalov, L. Tiator, Eur. Phys. J. A 34 (2007) 69, http://dx.doi.org/10.1140/epja/i2007-10490-6.

[11] E.D. Bloom, et al., Phys. Rev. Lett. 30 (1973) 1186, http://dx.doi.org/10.1103/PhysRevLett.30.1186.

[12] A.S. Esaulov, A.M. Pilipenko, Yu.I. Titov, Nucl. Phys. B 136 (1978) 511, http://dx.doi.org/10.1016/0550-3213(78)90273-0.

[13] E. Amaldi, et al., Phys. Lett. B 41 (1972) 216, http://dx.doi.org/10.1016/0370-2693(72)90465-0.

[14] P. Brauel, et al., Phys. Lett. B 45 (1973) 389, http://dx.doi.org/10.1016/0370-2693(73)90062-2.

[15] P. Joos, et al., Phys. Lett. B 62 (1976) 230, http://dx.doi.org/10.1016/0370-2693(76)90514-1.

[16] A. del Guerra, et al., Nucl. Phys. B 99 (1975) 253, http://dx.doi.org/10.1016/0550-3213(75)90004-8.

[17] A. del Guerra, et al., Nucl. Phys. B 107 (1976) 65, http://dx.doi.org/10.1016/0550-3213(76)90191-7.

[18] S. Choi, et al., Phys. Rev. Lett. 71 (1993) 3927, http://dx.doi.org/10.1103/PhysRevLett.71.3927.

[19] K. Park, et al., Phys. Rev. C 85 (2012) 035208, http://dx.doi.org/10.1103/PhysRevC.85.035208.

[20] K.I. Blomqvist, et al., Z. Phys. A 353 (1996) 415, http://dx.doi.org/10.1007/BF01285153.

[21] A. Liesenfeld, et al., Phys. Lett. B 468 (1999) 20, http://dx.doi.org/10.1016/S0370-2693(99)01204-6.

[22] D. Drechsel, L. Tiator, J. Phys. G 18 (1992) 449, http://dx.doi.org/10.1088/0954-3899/18/3/004.

[23] M.N. Rosenbluth, Phys. Rev. 79 (1950) 615, http://dx.doi.org/10.1103/PhysRev.79.615.

[24] K.I. Blomqvist, et al., Nucl. Instrum. Methods Phys. Res., Sect. A 403 (1998) 263, http://dx.doi.org/10.1016/S0168-9002(97)01133-9.

[25] D. Baumann, et al. (to be published).

[26] H. Herminghaus, et al., Nucl. Instrum. Methods 138 (1976) 1, http://dx.doi.org/10.1016/0029-554X(76)90145-2.

[27] http://wwwkph.kph.uni-mainz.de/MAID/maid.html.

[28] S.S. Kamalov, et al., Phys. Lett. B 522 (2001) 27, http://dx.doi.org/10.1016/S0370-2693(01)01241-2.

[29] S.S. Kamalov, et al., Phys. Rev. C 64 (2001) 032201(R), http://dx.doi.org/10.1103/PhysRevC.64.032201.

[30] S.S. Kamalov, S.N. Yang, Phys. Rev. Lett. 83 (1999) 4494, http://dx.doi.org/10.1103/PhysRevLett.83.4494.

[31] S.N. Yang, S.S. Kamalov, L. Tiator, AIP Conf. Proc. 1432 (2012) 293, http://dx.doi.org/10.1063/1.3701233.

[32] S.N. Yang, JPS Conf. Proc. 10 (2016) 042002, http://dx.doi.org/10.7566/JPSCP.10.042002.

[33] M. Hilt, B.C. Lehnhart, S. Scherer, L. Tiator, Phys. Rev. C 88 (2013) 055207, http://dx.doi.org/10.1103/PhysRevC.88.055207.

[34] M. Hilt, B.C. Lehnhart, S. Scherer, L. Tiator, JPS Conf. Proc. 10 (2016) 010007, http://dx.doi.org/10.7566/JPSCP.10.010007.

[35] F. James, Statistical Methods in Experimental Physics, 2nd edition, World Scientific, 2006.